Optical and magneto-optical properties and electronic structures of single-crystalline $R\mathrm{Al}_2$ (R=Y, La, Ce, Pr, and Lu)

R. J. Lange,* S. J. Lee,† K. J. Kim,‡ P. C. Canfield, and D. W. Lynch§
Ames Laboratory and Department of Physics and Astronomy, Iowa State University, Ames, Iowa 50011
(Received 1 May 2000; revised manuscript received 18 October 2000; published 29 December 2000)

The diagonal optical conductivity spectra of single crystals of $R\mathrm{Al}_2$ (R=Y, La, Ce, Pr, and Lu) were measured at room temperature by spectroscopic ellipsometry in the 1.5–5.6-eV range. All the compounds exhibit two strong interband absorption peaks at about 1.8 and 3.6 eV for YAl_2 and LuAl_2, and at about 2.0 and 3.0 eV for LaAl_2, CeAl_2, and PrAl_2. Such differences in the second peak position appear in the theoretical optical conductivity spectra calculated from their band structures obtained by the tight-binding linear-muffin-tin-orbitals method. Most of the contributions to the two peaks in LaAl_2 are from the p and d states, i.e., $p \rightarrow d$ and $d \rightarrow p$ transitions, while those involving f states are negligible. These results suggest that f character near E_F for LaAl_2, CeAl_2, and PrAl_2 distorts their conduction bands significantly through hybridization, leading to different optical spectra compared to those of YAl_2 and LuAl_2. The magneto-optical properties of CeAl_2 and PrAl_2 were measured at low temperatures. The Kerr rotation (Θ_K) and ellipticity (ϵ_K) for both compounds show similar spectral variations with maximum Θ_K of 0.35° and 0.55° at about 2.1 eV for CeAl_2 and PrAl_2, respectively. The evaluated off-diagonal conductivity spectra of the two compounds are also similar, with two structures at about 2.1 and 3.8 eV for CeAl_2 and 2.1 and 3.4 eV for PrAl_2. The energy difference in the second structures is interpreted as due to the different conduction-band structures of the two compounds caused by different hybridization strengths of their f states with conduction bands, because of the difference in their degree of localization.

DOI: 10.1103/PhysRevB.63.035105 PACS number(s): 78.20.Ls, 71.20.Eh, 75.60.Ej

I. INTRODUCTION

Rare-earth and transition-metal dialuminides have been investigated extensively because of a variety of interesting physical properties they exhibit, such as magnetism,[1–4] superconductivity,[5,6] the de Haas–van Alphen (dHvA) effect,[7] and thermal[8] and electronic properties.[9–17] Most of the compounds crystallize in the cubic Laves (MgCu_2) structure, in which the rare-earth or transition-metal atoms are arranged in the diamond structure consisting of two fcc lattices displaced from each other by one-fourth of a body diagonal, and the Al atoms are on sites of rhombohedral symmetry ($\bar{3}m$) in tetrahedra, with four rare-earth or transition-metal atoms as next-nearest neighbors. During the last decades nonmagnetic dialuminides such as YAl_2, LaAl_2, and LuAl_2 have been extensively studied both theoretically and experimentally.[10,11,14,17–19] These compounds are reference materials for studying $4f$-electron systems, because their $4f$ states are located well above, near, and well below the Fermi level E_F respectively. They are also important as host materials for doping with magnetic impurities. On the other hand, CeAl_2 and PrAl_2 show magnetic ordering. CeAl_2 orders antiferromagnetically below 3.8 K, and shows a strong competition between magnetic order and the Kondo effect, favoring a nonmagnetic singlet ground state.[20,21] PrAl_2 is a ferromagnet with T_C=33 K.[22,23]

Reichelt and Winzer[7] measured the dHvA effect in single crystals of LaAl_2, and compared the results with its calculated electronic band structure. They found good agreement between theory and experiment, and proposed a Fermi surface for LaAl_2. Jarlborg *et al.*[17] calculated the band structure of CeAl_2 and LaAl_2 self-consistently using the linear muffin-tin orbital (LMTO) method, neglecting spin-orbit coupling. They paid special attention to the role of the f-electron states in CeAl_2 and LaAl_2 in determining the electronic structure around E_F. Their calculation showed that the f bands in CeAl_2 are located near E_F, while those in LaAl_2 are located at 3 eV above it. The f states from La and Ce sites of the compounds were found to modify the s-p-electron configurations on the Al sites. They also showed that an antiferromagnetic state is stable in CeAl_2, and is favored over a ferromagnetic state. The band structure of LaAl_2 was also calculated by Hasegawa and Yanase[11] using the augmented-plane-wave (APW) method. They showed that the f bands in LaAl_2 above E_F distort the conduction band appreciably, and that the resultant Fermi surface could explain the experimental dHvA data reasonably well. Switendick[10] calculated the band structures of YAl_2, LaAl_2, and LuAl_2 using a nonrelativistic APW method. He concluded that there is considerable f character mixed in the conduction bands states near E_F in LaAl_2.

Spectroscopic ellipsometry (SE) was widely used to investigate optical properties and the related electronic structures of solids by measuring the change in the polarization state of light upon reflection at a sample surface. However, SE data on rare-earth and transition-metal dialuminide ($R\mathrm{Al}_2$) compounds are rare. Kim and Lynch[24] measured the optical properties of polycrystalline CeAl_2 and LuAl_2 using SE and reflectivity measurements in the 0.04–4.5-eV region to study the contributions of f states in the interband optical transitions. They found that the optical conductivity of CeAl_2 has structures at 0.1 and 1.0 eV, while LuAl_2 has no structure below 1 eV. The differences in optical conductivity between CeAl_2 and LuAl_2 were interpreted as originating from

 ©2000 The American Physical Society

the difference in electronic structure caused by the location of their f states. In $CeAl_2$, the f states are expected to be located near E_F, while for $LuAl_2$, they are well below it. Therefore, for $CeAl_2$ the f states may contribute to interband transitions at infrared frequencies, while for $LuAl_2$ interband transitions involving the f states can occur only at higher energies. Lee *et al.*[16] compared the measured optical spectra of single crystals of $YbAl_2$ and $LuAl_2$ with the theoretical optical conductivities obtained by the tight-binding linear muffin-tin-orbital (TB-LMTO) calculations under the atomic sphere approximation. The theoretical optical conductivity of $YbAl_2$ has strong peaks near 0.5 eV, while that of $LuAl_2$ shows no such feature in the same energy region, which is interpreted as due to interband transitions involving f states located near E_F for $YbAl_2$.

To investigate the effects of the f states on the electronic structures near E_F, we have grown single crystals of $LaAl_2$, $CeAl_2$, and $PrAl_2$, and compared their experimental optical conductivity spectra with those of YAl_2 and $LuAl_2$ single crystals as reference materials. The valence electronic configuration of Y is $4d^15s^2$, while that of La is $5d^16s^2$. The $4f$ states of Y in YAl_2 are located far above E_F. $LuAl_2$ differs from $LaAl_2$ in that elemental La has no $4f$ valence electrons while $LuAl_2$ has fully occupied $4f$ states well below E_F. Since the $4f$ states in YAl_2 and $LuAl_2$ are not expected to contribute to the optical transitions in the present spectral range (1.5–5.6 eV), we expect similar optical properties for YAl_2 and $LuAl_2$. For $CeAl_2$ and $PrAl_2$ magneto-optical Kerr effect (MOKE) spectra were also measured to investigate their magneto-optical properties and to obtain the off-diagonal components of their optical conductivity tensors induced by their magnetic properties. Any difference observed in the optical conductivity spectra of $LaAl_2$, $CeAl_2$, and $PrAl_2$, compared to those of YAl_2 and $LuAl_2$, is expected to be primarily due to the presence of their f states near E_F. To obtain the electronic structures and theoretical optical conductivity, including the off-diagonal component needed to interpret MOKE spectra of the compounds, the TB-LMTO method with the local density approximation (LDA) was employed. It is well known that the TB-LMTO method works well for the cubic Laves structure because they have closely packed structures with high symmetry.[14] The band structures, density of states, and theoretical optical conductivities were obtained for YAl_2, $LaAl_2$, and $LuAl_2$, and used to interpret the interband-transition structures in their experimental optical conductivities.

II. EXPERIMENTS

A. Sample preparation

Single crystals of YAl_2, $LaAl_2$, $CeAl_2$, $PrAl_2$, and $LuAl_2$ were prepared via two different flux-growth techniques.[25] For YAl_2, 45 and 55 mol % of elemental Y and Al, respectively, were placed in a sealed Ta crucible which was placed in a sealed quartz tube under a partial pressure of argon. Quartz wool was filled in the crucible and inverted over the top of the packed crucible. This assembly then was heated to 200 °C in 1 h, to 1350 °C in 8 h, held for 1 h, raised to 1480 °C in 2 h, then slowly cooled to 1200 °C over 120 h. The crystal grew during the first cooling step. At the temperature of 1200 °C, the sample was inverted and spun in a centrifuge, forcing the still-liquid flux out through the quartz wool and leaving the crystal in the crucible. The quartz wool in the crucible acts as the filter during flux removal. In the case of $LaAl_2$, $CeAl_2$, $LuAl_2$, and $PrAl_2$, elemental La, Ce, and Pr are mixed with Al in the same mol %. Each mixture was placed in a sealed Ta crucible which was placed in a sealed quartz tube, then heated to 1200 °C and slowly cooled to 890 °C, at which temperature the crystals were removed with the same method used for YAl_2. These crystals were octahedral, with typical dimensions of $3\times3\times3$ mm^3. However, when applied to $LuAl_2$, this technique produces small, intergrown crystals. Hence $LuAl_2$ was grown from a third-element flux, indium. The ternary melt was cooled slowly to 725 °C, at which temperature the crystals were removed from the flux. These crystals were larger than those produced from the binary melt, and had both octahedral and platelike morphologies. In the case of the platelike samples, the growth direction is along the [111] direction.

The surfaces of the YAl_2 and $LaAl_2$ single crystals looked somewhat dim due to the remnant flux on them. We used an alumina abrasive of 0.05-μm diameter to remove any possible remnant flux on the surfaces. The surfaces became mirrorlike after polishing several minutes, and did not need further treatment. The surface of the $LaAl_2$ crystal was clean and mirrorlike, so no further surface treatment was necessary before optical measurements. In the case of $CeAl_2$ and $PrAl_2$ the crystals showed no clean facets, unlike $LaAl_2$. These crystals are not so reactive, and so were polished, using silicon carbide spray with grades of 6, 1, and 0.25 μm, and rinsed with acetone and isopropanol. X-ray powder diffraction patterns of YAl_2, $LaAl_2$, and $LuAl_2$ were obtained from crushed single crystals, and lattice constants of YAl_2, $LaAl_2$, $CeAl_2$, $PrAl_2$, and $LuAl_2$ of 7.856, 8.155, 8.059, 8.024, and 7.747 Å, respectively, were determined. The lower limit for the detection of second phases in x-ray patterns is generally a few percent for the samples, and none were found.

B. Ellipsometry

The optical conductivities of the present compounds were measured by a rotating-analyzer-type SE in the 1.5–5.6-eV range. The principle of ellipsometry is the change in state of polarization of light upon reflection from the surface of a material. This change is directly related to the dielectric function of the reflecting material. The absorptive part of the dielectric function (ϵ_2) is related to the absorptive part of the optical conductivity (σ_1) by

$$\epsilon_2=\frac{4\pi\sigma_1}{\omega}. \tag{1}$$

The dielectric function or the optical conductivity is closely related to the electronic structure of the material. Using ellipsometry,[26,27] one measures the ratio of the complex

Fresnel reflection coefficients, r_p and r_s, for light polarized parallel (p) and perpendicular (s) to the plane of incidence respectively,

$$\tilde{\rho}=\frac{r_p}{r_s}=\left|\frac{r_p}{r_s}\right|e^{i\Delta}=\tan\Psi e^{i\Delta}=\frac{\sin^2\phi-\cos\phi\sqrt{\tilde{\epsilon}-\sin^2\phi}}{\sin^2\phi+\cos\phi\sqrt{\tilde{\epsilon}-\sin^2\phi}}, \tag{2}$$

where Ψ and Δ express the amplitude ratio and phase difference between the p and s components of polarized light reflected from a surface at an angle ϕ. Ψ and Δ are quantities directly measurable from ellipsometry, from which the complex dielectric function of the reflecting material can be determined.

C. Magneto-optic Kerr effect

Magneto-optical properties (polar Kerr effect) of $CeAl_2$ and $PrAl_2$ were measured by MOKE measurements at low temperatures ($T\leqslant 70$ K) in an optical cryostat. A split-coil superconducting magnet system enclosed in the cryostat can produce magnetic field up to 70 kOe. We used an intensity method employing a photoelastic modulator,[28,29] which affords simultaneous measurement of the two magneto-optical parameters, Kerr rotation, θ_K, and ellipticity, ϵ_K, with high accuracy. The principle of the technique, calibration, and other experimental details were described in detail elsewhere.[28–31] The off-diagonal components of the optical conductivity are related to the magneto-optical parameters (θ_K and ϵ_K) by[32]

$$\sigma_{1xy}=\frac{\omega}{4\pi}(-A\theta_K+B\epsilon_K),$$
$$\sigma_{2xy}=-\frac{\omega}{4\pi}(B\theta_K+A\epsilon_K), \tag{3}$$

where A and B are given by

$$A=-k^3+3n^2k-k,$$
$$B=-n^3+3k^2n+n. \tag{4}$$

The optical constants n and k of the samples are obtained by SE at room temperature.

III. BAND-STRUCTURE CALCULATIONS

We used the lattice constants from x-ray powder diffraction. The exchange-correlation potential was included in the local-density approximation with the von Barth–Hedin form.[33] The k-integrated functions were evaluated by the tetrahedron technique with 144 k points in the irreducible Brillouin zone, which is $\frac{1}{48}$ of the Brillouin zone. Once the self-consistent potential and the charge density were obtained, the real part of the optical conductivity was calculated. In cubic systems only one of the three equal diagonal components of the conductivity tensor needs to be calculated. We used Kubo's linear-response theory,[34] which leads to interband contributions to the conductivity of the form

$$\sigma_{xx}=\frac{\pi e^2}{3m^2\omega}\sum_{f,i}\int_{BZ}d^3k\frac{2}{(2\pi)^2}|p_{fi}|^2\times f_i(k)\times[1-f_f(k)]\times\delta[E_f(k)-E_i(k)-\hbar\omega], \tag{5}$$

where BZ denotes the Brillouin zone, $f(k)$ is the Fermi distribution function, and i and f stand for the occupied initial and unoccupied final energy-band states at wave vector **k**, respectively.

$$p_{fi}=\frac{\hbar}{i}\langle f|\nabla|i\rangle \tag{6}$$

is the dipole matrix element between the occupied and unoccupied one-electron states. The calculated spectra are unbroadened quantities. The electrons generally interact with other electrons. These correlated electrons are described by the quasiparticle picture using a self-energy correction. This self-energy ($\Sigma=\Sigma_1+i\Sigma_2$) is, in general, momentum and energy dependent. The real part of the self energy represents a shift of the one-electron energy, and the imaginary part describes the broadening of the energy level caused by the finite lifetime of a state. To take into account the finite lifetime of the excited quasiparticle state, the theoretical optical conductivity is convoluted with an energy-dependent Lorentzian broadening function[35] of width equal to the imaginary part of the complex self-energy, which was set empirically to $\Sigma_2(E)=0.1E$, where E is the incident photon energy.

IV. RESULTS AND DISCUSSION

A. Optical properties

The measured real parts of the room-temperature optical conductivity spectra of RAl_2 (R=Y, La, Ce, Pr, and Lu) are exhibited in Fig. 1. The conductivity spectra for YAl_2 and $LuAl_2$ are similar to each other in the peak positions of their two strong structures, as well as in their overall spectral shapes. The first peaks are located at about 1.8 eV for both compounds and the second peaks at about 3.6 and 3.8 eV for YAl_2 and $LuAl_2$, respectively. On the other hand, the optical conductivity spectra of $LaAl_2$, $CeAl_2$, and $PrAl_2$ are somewhat different from those of YAl_2 and $LuAl_2$. The first peaks of $LaAl_2$, $CeAl_2$, and $PrAl_2$ appear at about 2.0 eV, higher than those of YAl_2 and $LuAl_2$ by about 0.2 eV and their second peaks at about 3.0 eV, lower by about 0.6 and 0.8 eV, respectively.

The calculated band structures along high-symmetry lines and densities of states (DOS's) for YAl_2 and $LaAl_2$ are shown in Figs. 2 and 3, respectively. A similar figure for $LuAl_2$ can be found in Ref. 16. Strong direct interband transitions from the occupied states to the unoccupied states across E_F, corresponding to the observed absorption peaks, are denoted by arrows in the band structure. The calculated band structures and densities of states for the three compounds show similar features below E_F. The two peaks in the density of states between 6 and 9 eV below the Fermi energy are due to the mixed Al-s and Al-p states for all three compounds. The occupied states between E_F and 4.0 eV below E_F are primarily due to the Al-p and Y-, Lu-, or La-d

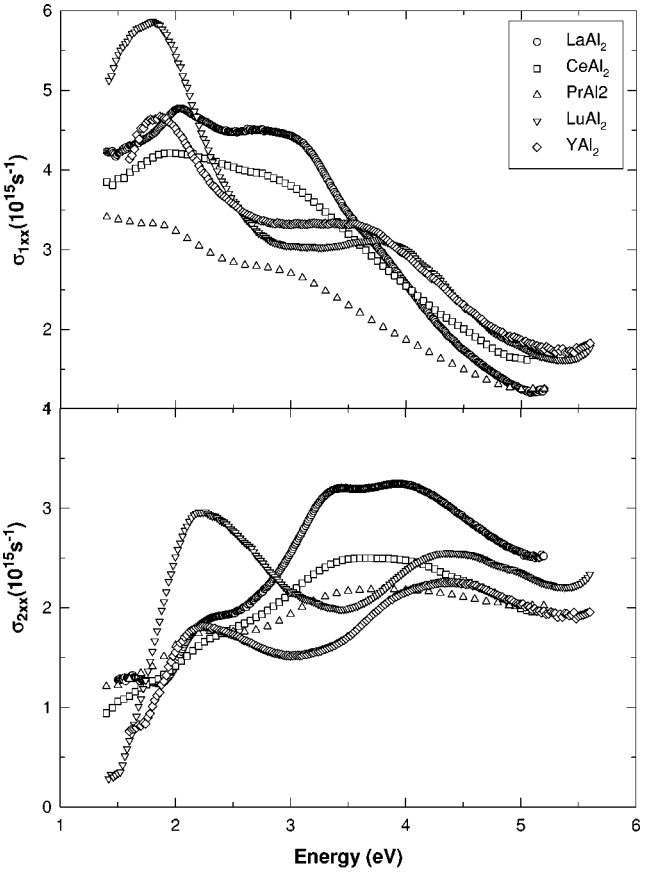

FIG. 1. Experimental optical conductivity spectra of RAl_2 (R = Y, La, Ce, Pr, and Lu).

states. The unoccupied f states of YAl_2 are located far above E_F, and are not shown in Fig. 3. For $LuAl_2$, two narrow f bands, separated by spin-orbit interaction, lie 4.0 and 5.5 eV below E_F. For $LaAl_2$, the unoccupied f bands are located around 3.0 eV above E_F. The DOS's at E_F, $N(E_F)$, for YAl_2, $LuAl_2$, and $LaAl_2$ are 42.90, 47.54, and 61.80 (states per Ry cell), respectively. $N(E_F)$ for $LaAl_2$ agrees well with that obtained by Jarlborg *et al.* (60 states per Ry cell).[17]

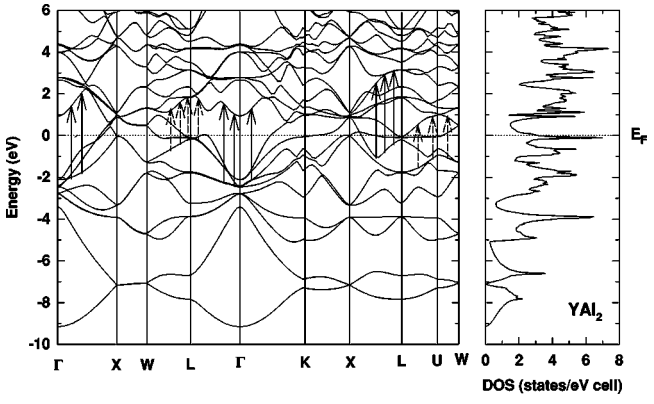

FIG. 2. Band structure along the high-symmetry lines and total density of states for YAl_2 obtained from the TB-LMTO method with the LDA in the atomic-sphere approximation, including spin-orbit splitting. Strong direct interband transitions corresponding to the measured peaks are marked by arrows.

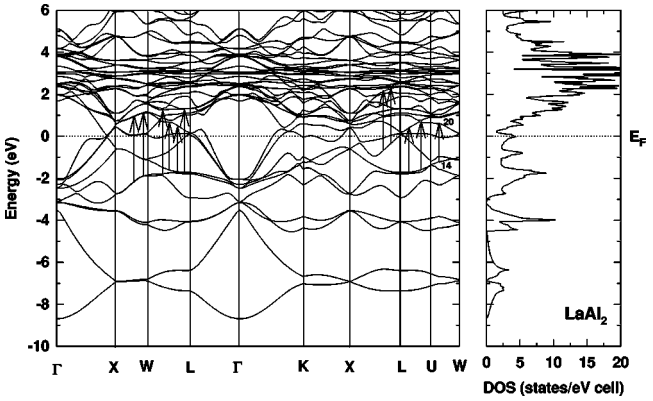

FIG. 3. Band structure along the high-symmetry lines and total density of states for $LaAl_2$ obtained from the TB-LMTO method with the LDA in the atomic-sphere approximation, including spin-orbit splitting. Strong direct interband transitions corresponding to the measured peaks are marked by arrows. Numbers 14 and 20 represent the transition band pair along the U-W line which contribute to the peak at 2.0 eV.

From the experimental electronic specific heat, one can estimate $N(E_F)$. The coefficient γ of the electronic specific heat is given by

$$\gamma = \frac{\pi^2}{3} N(E_F) k_B^2 (1 + \lambda + \mu), \tag{7}$$

where k_B is Boltzmann's constant, and λ and μ the mass enhancement factor due to electron-electron and electron-phonon interactions, respectively. The experimental electronic specific-heat coefficients γ of YAl_2, $LaAl_2$, and $LuAl_2$ were reported to be 5.46, 9.55, and 5.60 $\mathrm{mJ\,K^{-2}\,mol^{-1}}$, respectively.[8,36] The theoretical values for these compounds (without λ and μ) are obtained to be 3.73, 5.37, and 4.08 $\mathrm{mJ\,K^{-2}\,mol^{-1}}$, respectively, from the present calculations. The theoretical values of γ are smaller than the experimental data for all the compounds. The discrepancy between them is largest for $LaAl_2$, which is interpreted as due to the underestimation of the f-state contribution to DOS at E_F by the TB-LMTO band calculation based on the LDA.

The calculated optical conductivity spectra obtained from the band structures of the three compounds are shown in Fig. 4. They were broadened as described above. The calculated spectra for YAl_2 and $LuAl_2$ agree well with the experimental spectra for the energy positions of the interband absorption structures as shown in Fig. 4. The first peak appears at about 2.0 eV for both compounds, and the second at about 3.6 and 3.8 eV for YAl_2 and $LuAl_2$, respectively, exactly reproducing the energy difference between the second absorption structures. For $LaAl_2$, the first peak appears at about 2.0 eV, as for the other two compounds, while the second appears at about 3.0 eV, and the shape of the spectrum is quite different from those of YAl_2 and $LuAl_2$, as is also seen in the experimental spectra.

The electronic configurations of elemental Y, Lu, and La are similar; they each have about one electron in their d bands. The physical properties of YAl_2, $LuAl_2$, and $LaAl_2$,

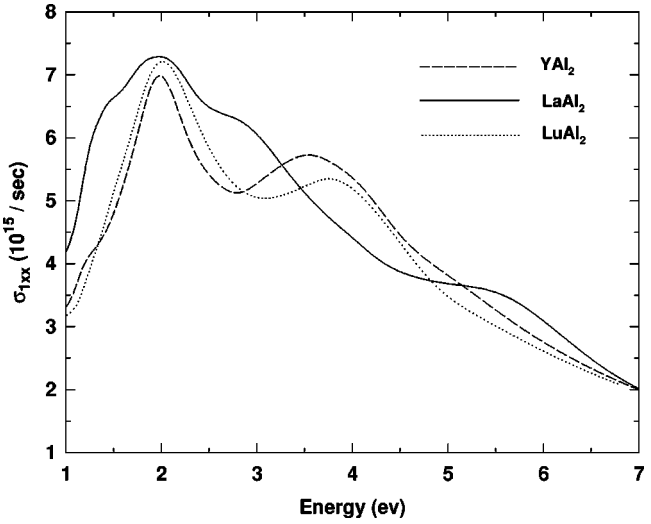

FIG. 4. Calculated optical conductivity spectra for YAl_2, $LaAl_2$, and $LuAl_2$ obtained from the TB-LMTO method using a lifetime broadening proportional to energy.

mainly related to their *d* bands, are expected to be similar. On the other hand, the *f* states in YAl_2 and $LuAl_2$ are not expected to affect the optical spectra in the present spectral range because they are located well above and below E_F for YAl_2 and $LuAl_2$, respectively. However, the *f* states in $LaAl_2$ near E_F can be strongly hybridized with neighboring conduction bands. Hasegawa and Yanase[11] showed that the *f* bands of $LaAl_2$ lie about 3.1 eV above E_F, and the other conduction bands near E_F are distorted significantly by them. Switendick[10] concluded that there is considerable *f* character mixed into the conduction bands near E_F in $LaAl_2$. However, there are no experimental optical data to prove such a prediction yet. As shown in Fig. 1, the optical conductivity spectrum of $LaAl_2$ looks quite different from those of YAl_2 and $LuAl_2$, reference compounds without *f* states near E_F. If the *f* states in $LaAl_2$ did not affect its band structure near E_F and the resultant optical spectrum in the present spectral range, its optical conductivity spectrum would be quite similar to those of YAl_2 and $LuAl_2$, which was not observed. Therefore, the *f* states in $LaAl_2$ at least cause a significant modification of the conduction bands through strong hybridization with *p*-*d* bands, leading to differences in the optical spectrum of the compound compared to those of YAl_2 and $LuAl_2$.

The identification of the band pairs contributing to the observed absorption peaks and their band characteristics are important to understand the origin of the absorption in the optical conductivity spectrum. This also informs us whether the unoccupied *f* states in $LaAl_2$ are directly involved in optical absorption through interband transitions or indirectly involved in it by changing the conduction bands located near them through hybridization. For the identification of band pairs which contribute most to the specific peak in the optical conductivity, all band pairs contributing to the peak were identified. In numbering bands, due to the degeneracy of spin-up and spin-down states for the paramagnetic YAl_2 and $LaAl_2$, one should double count each band. The initial and final band characters participating in the interband transitions should satisfy the selection rule $\Delta l = \pm 1$. For $LaAl_2$, the first strong peak at 2.0 eV is dominated by interband transitions between occupied bands (14–16) to unoccupied bands (22–24). The transition band pairs are 14→20, 14→22, 15→23, and 16→24. The occupied bands have Al-*p* and La-*p* characters hybridized with *d* bands. The unoccupied bands have La-*d* character hybridized with *p* bands and also Al-*p* character hybridized with *d* bands. The transitions around 2.0 eV occur near the lines *W*-*L*, *L*-*U*, and *U*-*W*, similar to the case of YAl_2. These transitions are marked as short dashed arrows in the electronic structure in Fig. 2. The peak at 3.0 eV comes from occupied bands (11–16) to unoccupied bands (26–34). The transition pairs are 11→26, 15→33, and 16→34. The transitions around 3.0 eV occur near the lines *X*-*W* and *W*-*L*. The occupied and unoccupied bands involved in the transition near 3.0 eV are primarily of La-*p* character hybridized with *d* bands. For the two peaks at 2.0 and 3.0 eV, there is no evidence for direct involvement of empty La-*f* states. But the different optical spectrum between 2.0 and 3.5 eV indicates that the conduction bands are distorted due to the presence of the *f* states. If the unoccupied La-*f* states were directly involved in interband transitions with the occupied La-*d* states, we can expect a spectrum different from those of YAl_2 and $LaAl_2$ above 3.5 eV. But the experimental spectra for three compounds above 3.5 eV are quite similar. Therefore, we can conclude that direct contributions of the La-*f* states to the optical conductivity can be ingored in the present spectral range.

B. Magneto-optic Kerr effects in $CeAl_2$ and $PrAl_2$

Paramagnetic YAl_2, $LaAl_2$, and $LuAl_2$ are expected to show barely detectable MOKE effects, so there has been no report of MOKE measurements. On the other hand, $CeAl_2$ and $PrAl_2$ show MOKE spectra, interpreted as mainly due to their partly filled *f* shells. Figure 5 shows the MOKE spectra for $CeAl_2$ and $PrAl_2$. Due to low light intensity it was not possible to obtain ellipticity data for $CeAl_2$ directly. We therefore used the Kramers-Kronig transform of the Kerr-angle spectra to calculate the ellipticity. Kerr-angle spectra for $CeAl_2$ were taken at 2.7 K with a 70-kOe magnetic field. Referring to Fig. 6, such a field is sufficient to induce ferromagnetic spin-alignment in the compound. In the case of $PrAl_2$ the ordering temperature is an order of magnitude higher than that of $CeAl_2$. We measured the MOKE spectra of $PrAl_2$ at 5 K and 10 kOe, sufficient to saturate $M(H)$ (Fig. 7). The spectra for both compounds are similar, showing a negative Kerr rotation, Θ_K, over the entire spectral range. Under the given conditions $PrAl_2$ has a magnetic moment that is at least a factor of three larger than that of $CeAl_2$. On the other hand, the amplitude of Θ_K of $PrAl_2$ is only about 1.5 times larger than that of $CeAl_2$. We note a first maximum in Θ_K at about 1.8 eV followed by a minimum at about 2.2 eV. These low-energy structures dominate the MOKE spectra in these compounds. At 3 eV we have a very weak peak in Θ_K which can be identified as a shoulder in the ellipticity data. There is another weak minimum at 3.8 eV. At higher energies Θ_K approaches zero.

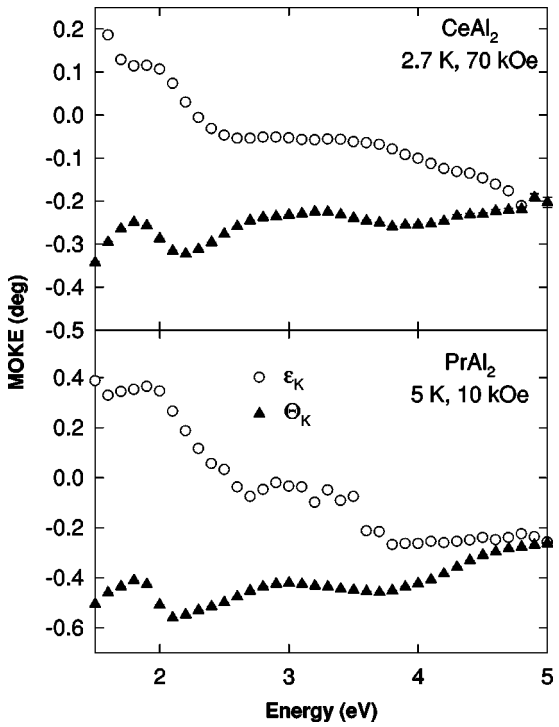

FIG. 5. Magneto-optic Kerr spectra of RAl_2 (R=Ce,Pr). ϵ_K for $CeAl_2$ was obtained from a Kramers-Kronig transformation of Θ_K.

Figure 8 shows the Kerr rotation versus magnetic field for $CeAl_2$. The upper panel shows data taken at the energy of minimum Θ_K in Fig. 5. For temperatures below T_N we have a very sharp metamagnetic transition to field-induced ferromagnetism. It should be noted that the spectra for 2.7 and 3.3 K are basically identical, whereas data taken at 2.1 K are clearly different. Θ_K at 2.1 K is smaller than at higher temperatures, which is attributable to stronger antiferromagnetic interactions at this temperature. Furthermore we note a decrease of Θ_K with increasing magnetic field. This is unusual, since $M(H)$ data indicate an increase of the magnetization, even at lower temperatures. Similar anomalies were observed in CeSb by Pittini *et al.*[37] Even at 7 K, which is above T_N, we can still identify the phase transition which is already too small to be detected in the magnetization data at 3.3 K (Fig. 6). Our Θ_K data show stronger saturation effects than those in $M(H)$, although a complete saturation of the Kerr rotation cannot be achieved up to 70 kOe. The lower panel of Fig. 8 shows data taken at 2.7 K at different photon energies. The curves are very similar, indicating the proportionality of the Kerr rotation to the spin polarization of the states involved in the transitions at 2.1 and 4.6 eV. The phase transition occurs between 40 and 50 kOe in $M(H)$, and around 30 kOe in the Kerr spectra. Since the anisotropy in this compound is small, we believe that this is due to different samples. The sample

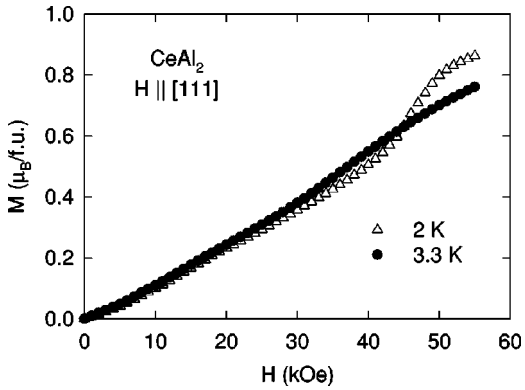

FIG. 6. Magnetic moment per Ce as a function of field with $H \| [111]$. We show one scan well below T_N=3.8 K, and another one very close to it.

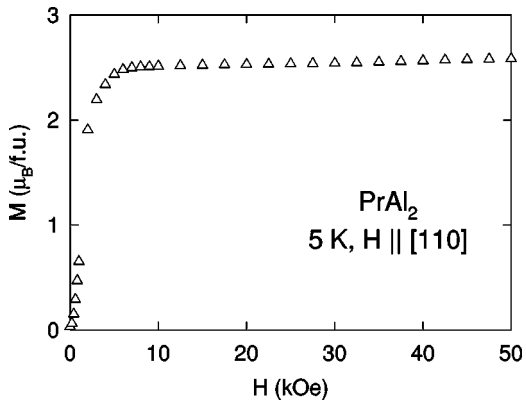

FIG. 7. Magnetization vs field for $PrAl_2$ with applied field along the [110] direction.

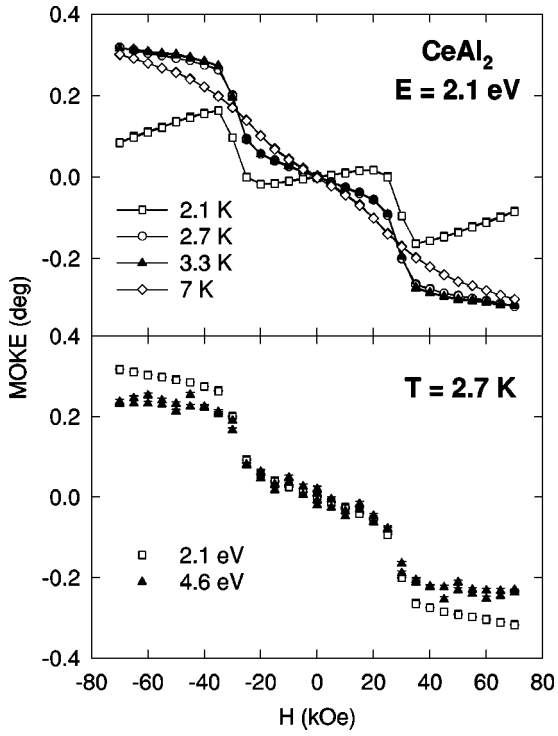

FIG. 8. Field dependence of the Kerr rotation of $CeAl_2$. Field scans at constant energy are shown in the upper panel. The metamagnetic transition to a field-induced ferromagnetic structure begins at 30 kOe. The lower panel shows the energy dependence of the saturation behavior of Θ_K below T_N.

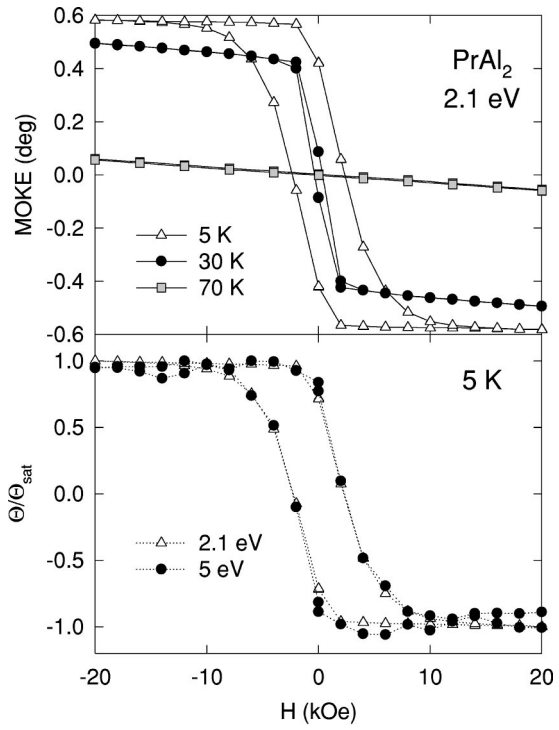

FIG. 9. Kerr rotation versus field for $PrAl_2$. Upper panel: MOKE at 2.1 eV at 5, 30, and 70 K. Lower panel: normalized Kerr rotation at 5 K at 2.1 and 5 eV.

used in the optical experiment is fairly large, and magnetization measurements could not be performed on this specimen.

Figure 9 shows similar scans for $PrAl_2$ at 2.1 eV. Below T_C we observe ferromagnetic behavior with an increasing hysteresis at lower temperatures. At 5 K, Θ_K saturates at nearly $-0.6°$ in an external field of 10 kOe. The Kerr rotation in this sample is proportional to the magnetization shown in Fig. 7. As expected, Θ_K is strongly reduced above the ordering temperature. In order to check the energy dependence of Θ_K we took Kerr loops at different energies. Figure 9 shows the normalized Kerr rotation and it is obvious that the transitions at both energies are of similar origin.

We calculated the absorptive part of the off-diagonal conductivity, $\omega\sigma_{2xy}$, from the experimental Kerr rotation and ellipticity and the measured diagonal optical conductivity σ_{1xx}, using Eq. (3). The intraband contributions by nearly free electrons to σ_{2xy} are expected to be proportional to ω^{-1}, shown in Fig. 10 as constant shifts at low energies below 2 eV for both compounds. Again the absorption spectra look very similar to each other. We can identify two peaks at about 2.1 and 3.8 eV in $CeAl_2$ and 2.1 and 3.4 eV in $PrAl_2$. Then absorption decreases toward higher energies, and there might be more transitions above 4.5 eV which produce a weak shoulder in σ_{2xy} for both compounds. Comparing the off-diagonal conductivity with the diagonal conductivity we expect that the structure at 2.1 eV is due to $p \rightarrow d$ transitions. The higher-energy peaks, which show a blueshift for $CeAl_2$ with respect to $PrAl_2$, are tentatively assigned to $d \rightarrow p$ transitions. $PrAl_2$ shows transitions which are very close in energy to those observed in heavier rare-earth compounds, so the blueshift of the second absorption peak in $CeAl_2$ in the

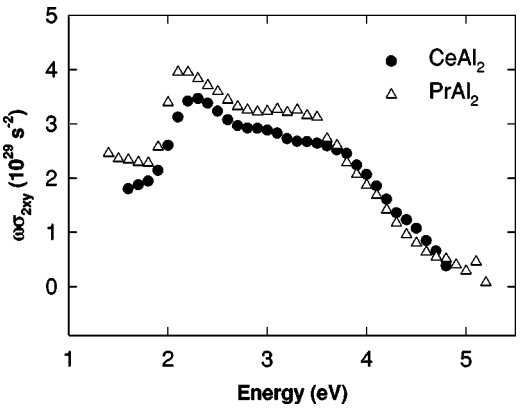

FIG. 10. Absorptive part of the off-diagonal optical conductivity of RAl_2 (R=Ce,Pr) calculated from the diagonal optical conductivity and the Kerr parameters.

$\omega\sigma_{2xy}$ is therefore associated with the special role of Ce in the compound. Strong hybridization involving f states, as evidenced by the Kondo effect and the reduced moment observed even at temperatures exceeding T_K in $CeAl_2$, is expected to give rise to stronger distortion of the conduction bands of the compound in the vicinity of E_F compared to $PrAl_2$. This leads to the observed shift of the second absorption peak in the experimental $\omega\sigma_{2xy}$, which might not be detected in the σ_{1xx} spectra due to its integrated nature.

V. SUMMARY AND CONCLUSIONS

The diagonal optical conductivity spectra of single-crystals of RAl_2 (R=Y, La, Ce, Pr, and Lu) were measured between 1.5 and 5.6 eV, and compared with the results of calculations using the self-consistent TB-LMTO method. The experimental optical conductivity spectra show two strong absorption structures for all the compounds. The first peaks are around 2.0 eV for all the compounds. The second peaks of $LaAl_2$, $CeAl_2$, and $PrAl_2$ are at about 3.0 eV, shifted to lower energies from those of YAl_2 and $LuAl_2$ by about 0.6 eV. The calculated optical conductivities of YAl_2, $LuAl_2$, and $LaAl_2$ show good agreement in the energy positions of their absorption structures with those of the experimental spectra. For the two peaks at 2.0 and 3.0 eV, it is found that the contribution of the empty f states is negligible. The f states of $LaAl_2$ do not give significant contributions to its optical conductivity from interband transitions but the distortion of the conduction bands due to the presence of the f states results in the difference in its optical spectrum, along with those of $CeAl_2$ and $PrAl_2$, compared to those of YAl_2 and $LuAl_2$ in the 2.0–3.5-eV range. The Kerr rotation Θ_K and ellipticity ϵ_K of $CeAl_2$ and $PrAl_2$ were measured at 2.7 K for $CeAl_2$ and 5 K for $PrAl_2$ under applied magnetic fields of 70 and 10 kOe for $CeAl_2$ and $PrAl_2$ respectively. The measured Θ_K and ϵ_K for both compounds show similar spectral variations with photon energy with their maximum Θ_K of 0.35° and 0.55° at about 2.1 eV for $CeAl_2$ and $PrAl_2$ respectively. The evaluated off-diagonal conductivity spectra of the two compounds also show a similarity with each other, with two strong peaks at about 2.1 and 3.8 eV for $CeAl_2$ and

2.1 and 3.4 eV for $PrAl_2$. The blueshift of the second peak of $CeAl_2$, compared to that of $PrAl_2$, is interpreted as being due to a greater degree of distortion of the conduction bands of $CeAl_2$ due to the presence of a stronger *f* character in them as compared to $PrAl_2$.

ACKNOWLEDGMENTS

Ames Laboratory is operated for the U.S. Department of Energy by Iowa State University under Contract No. W-7405-Eng-82. This work was supported by the Director for Energy Research, Office of Basic Energy Science.

*Present address: Philips Research Laboratory, Eindhoven, the Netherlands.

†Present address: Metals Development, Ames Laboratory, Ames, Iowa 50011.

‡Permanent address: Department of Physics, Konkuk University, Seoul 143-701, Korea.

§Author to whom correspondence should be addressed. Electronic address: dwl@ameslab.gov

[1] Y.B. Barash and J. Barak, J. Phys. F: Met. Phys. **14**, 1531 (1984).

[2] J.S. Abell, J.X. Boucherle, R. Osborn, B.D. Rainford, and J. Schweizer, J. Magn. Magn. Mater. **31**, 247 (1983).

[3] E.W. Lee and J.F.D. Montenegro, J. Magn. Magn. Mater. **22**, 282 (1981).

[4] G. Chelkowska, J. Magn. Magn. Mater. **127**, L37 (1993).

[5] B. Vlcek, E. Seidi, and H.W. Weber, Jpn. J. Appl. Phys. **26**, 967 (1987).

[6] J.R. Cooper, Solid State Commun. **9**, 1429 (1971).

[7] J. Reichelt and K. Winzer, Phys. Status Solidi B **89**, 489 (1978).

[8] C.A. Luengo and M.B. Maple, Solid State Commun. **12**, 757 (1973).

[9] R. Stiller, H. Merz, W. Drewes, and H.-G. Purwins, J. Phys. (Paris), Colloq. **9**, C-997 (1987).

[10] A. C. Switendick, in *Proceedings of the 10th Rare Earth Res. Conference (Carefree, Arizona) 1973*, edited by C. J. Kevane and T. Moeller (U.S. Atomic Energy Commission, Oak Ridge, TN 1973), Vol. 1, p. 235.

[11] A. Hasegawa and A. Yanase, J. Magn. Magn. Mater. **15**, 887 (1980).

[12] M. Magnitskaya, G. Chelkowska, G. Borstel, M. Neumann, and H. Ufer, Phys. Rev. B **49**, 1113 (1994).

[13] Yu.P. Smirnov, A.E. Sovestnov, G.I. Terekhov, A.V. Tyunis, and V.A. Shaburov, Fiz. Tverd. Tela (Leningrad) **30**, 3513 (1988) [Sov. Phys. Solid State **30**, 2021 (1988)].

[14] T. Jarlborg, A.J. Freeman, and D.D. Koelling, J. Appl. Phys. **53**, 2140 (1982).

[15] W.E. Pickett and B.M. Klein, J. Less-Common Met. **93**, 219 (1983).

[16] S.J. Lee, S.Y. Hong, I. Fisher, P.C. Canfield, B.N. Harmon, and D.W. Lynch, Phys. Rev. B **61**, 10 076 (2000).

[17] T. Jarlborg, A.J. Freeman, and D.D. Koelling, J. Magn. Magn. Mater. **60**, 291 (1986).

[18] B. Frick and M. Loewenhaupt, Physica B & C **130**, 372 (1985).

[19] A. Slebarski, E. Zipper, and J. Auleytner, J. Phys. F: Met. Phys. **13**, 2643 (1983).

[20] R.W. Hill and J.M. Machado da Silva, Phys. Lett. A **30**, 13 (1969).

[21] B. Barbara, J.X. Boucherle, J.L. Buevoz, M.F. Rossignol, and J. Schweizer, Solid State Commun. **24**, 481 (1977).

[22] N. Nereson, C. Olson, and G. Arnold, J. Appl. Phys. **39**, 4605 (1968).

[23] H.G. Purwins, E. Walker, B. Barbara, M.F. Rossignol, and P. Bak, J. Phys. C **7**, 3573 (1974).

[24] K.J. Kim and D.W. Lynch, J. Phys.: Condens. Matter **5**, 5971 (1993).

[25] P.C. Canfield and Z. Fisk, Philos. Mag. B **65**, 1117 (1992).

[26] R. M. A. Azzam and N. M. Bashara, *Ellipsometry and Polarized Light* (North-Holland, Amsterdam, 1977).

[27] D.E. Aspnes and A.A. Studna, Appl. Opt. **14**, 220 (1975).

[28] K. Sato, Jpn. J. Appl. Phys. **20**, 2403 (1981).

[29] K. Sato, H. Hongu, H. Ikekame, Y. Tosaka, M. Watanabe, K. Takanashi, and H. Fujimori, Jpn. J. Appl. Phys. **32**, 989 (1993).

[30] W.S. Kim, M. Aderholz, and W. Kleemann, Meas. Sci. Technol. **4**, 1275 (1993).

[31] S. J. Lee, Ph.D. thesis, Iowa State University, 1998.

[32] J. Schoenes and W. Reim, J. Magn. Magn. Mater. **54**, 1371 (1986).

[33] U. von Barth and L. Hedin, J. Phys. C **C5**, 1629 (1972).

[34] R. Kubo, J. Phys. Soc. Jpn. **12**, 570 (1957).

[35] J.E. Müller, O. Jepsen, and J.W. Wilkins, Solid State Commun. **42**, 365 (1982).

[36] R.E. Hungsberg and K.A. Gschneidner, Jr., J. Phys. Chem. Solids **33**, 401 (1972).

[37] R. Pittini, J. Schoenes, and P. Wachter, J. Magn. Magn. Mater. **177-181**, 472 (1998).